

Freeze–thaw cycles for biocompatible, mechanically robust scaffolds of human hair keratins

Xinxing Cui,^{1†} Songmei Xu,^{1†} Wen Su,¹ Zhe Sun,¹ Zeng Yi,¹ Xiaomin Ma,¹ Guangcan Chen,¹ Xiangyu Chen,¹ Bo Guo,² Xudong Li¹

¹National Engineering Research Center for Biomaterials, Sichuan University, Chengdu, 610064, People's Republic of China

²Department of Ophthalmology, West China Hospital, Sichuan University, Chengdu, 610041, People's Republic of China

Received 26 April 2018; revised 19 August 2018; accepted 23 August 2018

Published online 19 October 2018 in Wiley Online Library (wileyonlinelibrary.com). DOI: 10.1002/jbm.b.34237

Abstract: The keratin-based scaffolds are getting more and more attention in the application of tissue engineering. Though various approaches have been considered to improve the physical properties of these scaffolds, few succeeded in achieving the enhanced properties of the pure keratin scaffolds. Due to the presence of –OH, –NH₂, >C=O, and –SH on the extracted human hair keratin (HHK), the formation of hydrogen bonds and disulfide bridges could be triggered under certain conditions, leading to the self-cross-linking of HHK materials. Herein, a simple and green strategy was introduced, *via* freeze–thaw cycles of keratin solutions without addition of extraneous reagents, to obtain the mechanically robust HHK scaffolds. The comparative quantitation of residual –SH among the samples treated with 1, 5, and 9 cycles confirmed the oxidation in the thaw process for forming disulfide bonds. So, the equivalent thaw time was applied in this study, and three groups of the treated samples after 1, 5, and 9 cycles with an appropriate extension thaw time were

prepared to solely investigate the effects of physical cross-linking networks, primarily by formation of hydrogen bonds, on the properties of the obtained scaffolds. The systematic assessments including swelling behavior, porosity, thermal analysis, compressive measurement, and microstructural observation confirmed that the repetitive freeze–thaw treatment contributed to mechanically robust scaffolds with good porous interconnectivity. The cell culturing experiments further verified that these HHK scaffolds had desirable cytocompatibility, permitting the proper proliferation, attachment, and infiltration. Accordingly, this study provided a simple and efficient method to obtain biocompatible, mechanically robust keratin scaffolds. © 2018 Wiley Periodicals, Inc. *J Biomed Mater Res Part B: Appl Biomater* 107B:1452–1461, 2019.

Key Words: human hair keratin, cross-linking, freeze–thaw, scaffolds

How to cite this article: Cui X, Xu S, Su W, Sun Z, Yi Z, Ma X, Chen G, Chen X, Guo B, Li X. 2019. Freeze–thaw cycles for biocompatible, mechanically robust scaffolds of human hair keratins. *J Biomed Mater Res Part B* 2019:107B:1452–1461.

INTRODUCTION

Hair is a naturally occurring material mainly composed by keratins.¹ As a functional protein, the keratin extracted from human hair contains several protein species carrying cell adhesion sequences such as Arg–Gly–Asp (RGD) and Leu–Asp–Val (LDV) that mimic the extracellular matrix.^{2–4} The salient features of human hair keratins (HHKs) are very attractive and thus HHK have been widely exploited for various biomedical purposes, such as nerve repairing,⁴ skin regeneration,^{5,6} hemostasis,^{7–9} and drugs delivery.^{10–12} Owing to the intrinsic nature of spontaneous self-assembly, keratins could be fabricated into films, sponges, fibers, and scaffolds to further meet the requirements of different applications.^{13,14}

Generally, the keratin-based scaffolds can be achieved directly by freeze-drying the dialyzed keratin solutions.^{2,3,15} However, the underlying weakness associated with this method is the relatively poor mechanical properties of the fabricated keratin scaffolds. In principle, porous scaffolds used as provisional templates in tissue repair and engineering should possess appropriate mechanical strengths and stable microstructures, so as to provide a physical support for cell adhesion and proliferation.^{16–18} Therefore, seeking for an efficient method to produce mechanically strong keratin-based scaffolds is of paramount importance and has received extensive attention.

Up to now, several approaches have been considered for enhancing the mechanical properties of keratin-based

[†]These authors contributed equally to this work.

Correspondence to: B. Guo; e-mail: guobohx@163.com or X. Li; e-mail: xli20004@yahoo.com

Contract grant sponsor: National Basic Research Program of China (973 Program); contract grant number: 2012CB933600

Contract grant sponsor: National Key Research and Development Program of China; contract grant number: 2016YFC1102700

Contract grant sponsor: Sichuan Science and Technology Program Key Projects; contract grant number: 2017JY0018

materials, including the addition of natural polymers such as gelatin,^{19,20} silk fibroin,^{21,22} chitosan,^{19,23} alginate,^{24,25} and the use of cross-linking agents such as ethylene glycol diglycidyl ether (EGDE),²⁶ dialdehyde starch,²⁷ and transglutaminase.²⁸ To a varying extent, these methods were reported to give more desirable keratin-based composite materials. However, to the best of our knowledge, without using any other materials or extraneous reagents, the biocompatible, mechanically robust scaffolds of pure keratins have not been reported yet.

Freeze–thaw cycles were used to enhance the physical properties of polymers, primarily by the formation of hydrogen bonds among the chemical groups of molecular chains during the cycles.²⁹ Such chemical groups as $-\text{NH}_2$, $-\text{OH}$, and $>\text{C}=\text{O}$ are abundant in keratin. Thus the physical cross-links *via* primarily hydrogen bonds are supposed to be formed by freeze–thaw cycles of the pure keratin solution³⁰ (Figure 1). Meanwhile, $-\text{SH}$ groups on keratin chains could also be oxidized into disulfide bonds³¹ (Figure 1). In contrast to the use of cross-linking agents which might bring the potential biotoxicity to organisms, the self-cross-linking networks *via* the formation of hydrogen bonds and disulfide bonds during freeze–thaw cycles are more appropriate for enhancing the physical properties of the pure keratin scaffolds while ensuring their excellent biocompatibility.

In this study, a green fabrication approach without adding any extraneous reagents or materials was introduced in the preparation of the pure HHK scaffolds. One, five, and nine freeze–thaw cycles were carried out to produce scaffolds with different degree of the cross-links *via* hydrogen bonds and disulfide bonds. To illustrate their effects on the properties of the obtained HHK scaffolds, the comprehensive assessments including swelling ratio, porosity, thermal stability, and compressive strength were conducted. Biocompatibility of the scaffolds was also evaluated by investigating the proliferation and infiltration of cells seeded on the HHK scaffolds.^{5,32}

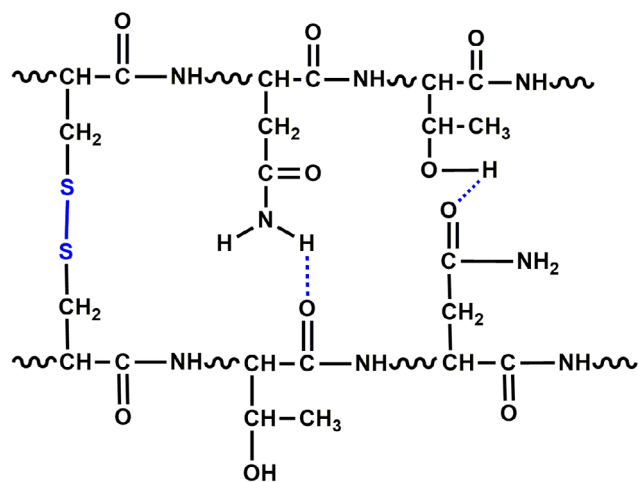


FIGURE 1. Schematic representation for self-cross-linking networks between two keratin chains *via* the formation of disulfide bridges from two cysteine residues and hydrogen bonds among $-\text{NH}_2$, $-\text{OH}$, and $>\text{C}=\text{O}$ during freeze–thaw cycles.

MATERIALS AND METHODS

Materials

Human hair was obtained from a local barber. Tris (hydroxy-methyl)-aminomethane, thiourea, urea, 2-mercaptoethanol, and 5'5'-dithiobis (2-nitrobenzoic acid) (DTNB) were commercially available. Dulbecco's modified eagle medium (DMEM, Gibco), trypsin, fetal calf serum, and penicillin-streptomycin antibiotics (Chengdu hali, China) were used in cell culture. Methyl thiazolyl tetrazolium (MTT), Rhodamine B isothiocyanate, Hoechst 33258, and Acridine orange (AO) were purchased from Sigma.

HHK extraction

The reduced HHK solution was prepared as previous reported.⁵ Briefly, human hair was cleaned with water and then air-dried; external lipids were removed by soaking the hair in a mixture of chloroform/methanol (2:1, v/v) at room temperature (RT) for 24 h. The delipidized hair (100 g) was immersed in a pH 8.5 solution (1 L) containing 25 mM Tris-HCl, 5 M urea, 2.6 M thiourea, and 5% 2-mercaptoethanol at 37°C for 3 days. After being filtered, the obtained mixture was centrifuged at 15,000 rpm for 20 min at RT. The supernatant was thoroughly dialyzed against distilled water using cellulose tubing (molecular mass cutoff 10 kDa) for 4 days (under N₂ atmosphere) and the dialysate was replaced with distilled water twice per day. The dialyzed keratin solution was collected and diluted to 20 mg/mL with distilled water, and then stored at 4°C as the stock solution for the following experiments.

Freeze–thaw cycles for HHK scaffolds

The flat-bottom tubes (1 cm in diameter) were used to contain HHK solution (20 mg/mL) during the freeze–thaw treatment. In each freeze–thaw cycle, the sample was frozen at –20°C for 24 h, and then thawed at 37°C for 4 h. 1, 5, and 9 freeze–thaw cycles were used to treat the HHK solutions, and the obtained three groups of samples were thus designated as HHK-gel/1, HHK-gel/5, and HHK-gel/9, respectively. The HHK solution without the freeze–thaw treatment was used as control. Considering that the oxidation of $-\text{SH}$ groups of keratins may occur in the thaw process, the equivalent thaw time to that applied in 9 freeze–thaw cycles was adopted. Therefore, varying extra thaw times were applied to the samples after different cycles, that is, 32 h for 1 cycle and 16 h for 5 freeze–thaw cycles. The obtained products were designated as HHK-gel/1 + 32 h, HHK-gel/5 + 16 h, and the lyophilized ones as HHK-scaffold/1 + 32 h, HHK-scaffold/5 + 16 h and HHK-scaffold/9 were collected for the following studies.

Quantitation of $-\text{SH}$ groups

The amount of the residual $-\text{SH}$ groups after freeze–thaw cycles of the HHK solutions was measured by using a DTNB assay.³³ Briefly, the DTNB standard solution was prepared by dissolving 0.5 mmol DTNB powder into 50 mL phosphate buffer solution (PBS). The DTNB working solution (0.1 mM) was prepared by diluting the DTNB standard solution with a 0.25 M Tris-HCl buffer solution (pH 8.3) and stored in the

dark at 4°C. After mixing 100 μL test samples with 9900 μL DTNB working solution and incubating 10 min at RT, the optical absorption value of the mixture was recorded by a UV-Vis spectrophotometer at 412 nm immediately. Each value was averaged on the basis of three parallel measurements.

Swelling measurement

The obtained HHK scaffolds were immersed in a sealed tube and filled with PBS. The samples were taken out when soaked for 2, 4, 8, 16, and 32 h at 37°C. After the surface liquid of the samples was removed by filter paper, the weight (W_{wet}) was recorded when the weight did not increase any more. The samples were lyophilized and then weighed (W_{dry}). The swelling ratio (SR) of the HHK scaffold was calculated according to the formula:

$$\text{SR} (\%) = (W_{\text{wet}} - W_{\text{dry}}) / W_{\text{dry}} \times 100\%$$

Each value was averaged on the basis of five parallel measurements.

Porosity measurement

The porosity of the HHK scaffolds was determined by the method of pycnometer at RT. Briefly, the scaffolds were weighed (W_0) and placed into a pycnometer filled with ethanol. Transferred into a vacuum oven until no bubbles were released from the system, the pycnometer was taken out and immediately weighed (W_1). Subsequently, the samples saturated with ethanol were taken out and the weight (W_2) of remaining ethanol and the pycnometer was recorded. The porosity of the HHK scaffold was calculated according to the formula:

$$P (\%) = (W_1 - W_2 - W_0) / (W_1 - W_2) \times 100\%$$

Each value was averaged on the basis of five parallel measurements.

Thermal analysis

To study the intermolecular interaction between keratin chains, the thermal stability of the HHK scaffolds was evaluated by using thermogravimetric analysis (TGA, STA 449C) under nitrogen atmosphere. The temperature range was from ambient temperature to 900°C and the heating rate was 10°C/min. About 7 mg of each sample was used in each test.

Compressive measurement

Three groups of the HHK scaffolds were tailored to about 15 mm thickness to obtain flat and parallel surfaces for compressive testing. Uniaxial compression was conducted at RT in dry conditions using a Universal mechanical tester (Shimadzu, Japan) with 50 kN load cell. The cross-head speed was set at 0.4 mm/min and the tests terminated when samples were compressed to ~40% strain.³⁴ The compressive modulus and compressive strength of scaffolds were computed from the slope of the linear region in the obtained stress-strain curves. Each value was averaged on the basis of five parallel measurements.

Microstructure observation

The scaffolds (1 mm in thickness) were mounted on aluminum stubs with conductive paint and were sputter-coated with gold. By using a Hitachi S-4800 scanning electron microscope (SEM) at an operation voltage of 3.0 kV, the microstructural morphology was examined.

Based on the autofluorescence of the HHK proteins, confocal laser scanning microscopy (CLSM) was used to further observe the distribution of micropores within the HHK scaffolds with laser lines at the excitation/emission wavelength of 488/534 nm. A series of 5-μm-thick slices along the z-axis were taken from the surface and downward to a depth of 500 μm, and thus the three-dimensional structures of the scaffolds were reconstructed by overlaying these slices.

Cell viability and behavior within the HHK scaffolds

The scaffolds (2 mm in thickness) were presterilized in 75% ethanol aqueous solution and washed by sterilized PBS. Then, the samples were immersed in DMEM and incubated at 37°C with 5% CO₂. NIH3T3 cells were seeded at the concentration of 3000 cells/scaffold in each well of cell culture plates. Fresh medium was replenished every 3 days. Cell viability was assessed by MTT assay at selected time points (7, 14, 21, and 28 days). Each value was averaged on the basis of five parallel measurements.

Cell proliferation and infiltration within the HHK scaffolds were observed by CLSM (Leica SP5). At 28 days, the cell-seeded scaffolds were fixed by 3.7% paraformaldehyde/PBS for 10 min, then washed three times with PBS, and finally stained with 5 μg/mL Hoechst 33258, Acridine orange, and Rhodamine B for 30 min at 37°C. A series of 5-μm-thick slices along the z-axis were taken from the top surface and downward to the max-depth of the visible cells infiltrating into scaffolds, and thus the three-dimensional structure of a cell-cultured scaffold was reconstructed. Meanwhile, the max-depth of the cell infiltration within scaffolds was measured based on the number of these slices.

Microstructure examination after cell culturing

The possible effect of the scaffold microstructure on the cell activity was assessed by using SEM. At 14 days of cell culturing, the scaffolds were fixed by 3.7% paraformaldehyde/PBS for 10 min. Then, samples were washed three times with PBS and freeze-dried. Hitachi S-4800 SEM at an operation voltage of 3.0 kV was used for observing these cell-cultured scaffolds.

RESULTS

Solution to gel with freeze-thaw cycles

As shown in Figure 2(A), the viscous semi-gel with relaxed structure was already formed in HHK-gel/1 + 32 h. For the HHK-gel/5 + 16 h [Figure 2(B)], the initial liquid-phase was transformed into a gel-phase. Comparably, the elastic hydrogel was achieved in HHK-gel/9 [Figure 2(C)]. However, the blank control still stayed at fluid state [Figure 2(D)]. The freeze-thaw cycles definitely accelerated the morphology transition of the HHK solution to HHK gel.

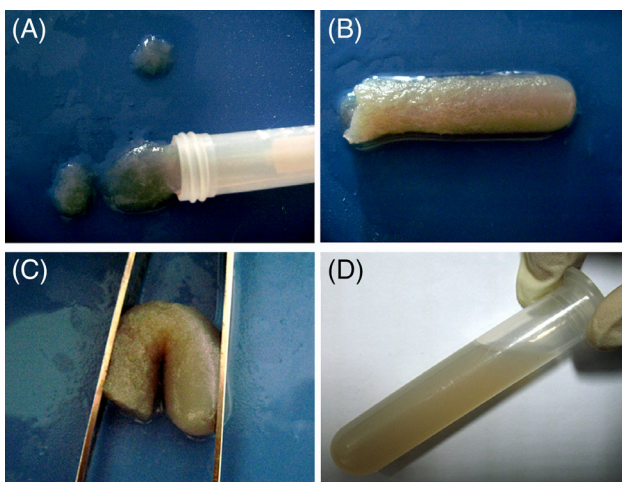


FIGURE 2. Comparative photographs of the HHK samples after different freeze-thaw cycles: (A) HHK-gel/1 + 32 h, (B) HHK-gel/5 + 16 h, (C) HHK-gel/9, and (D) the control (without freeze-thawing cycle).

Quantitation of -SH groups

In this experiment, the amount of the -SH groups in the stock solution was set as the 100% free -SH. As presented in Figure 3, a large amount of -SH groups still existed in the HHK-gel/1 (77%) and HHK-gel/5 (51%). But with a varying extension of thawing time, the residual amounts of -SH groups in the HHK-gel/1 + 32 h and HHK-gel/5 + 16 h reduced to about 10% of the stock solution, showing no significant difference with the groups remained in HHK-gel/9. The results indicated that the thawing process led to the effective consumption of -SH groups by oxidation to disulfide bonds.

Swelling behaviors

As exhibited in Figure 4(A), the SR of all the HHK scaffolds increased quickly in the first 4 h of incubation. The HHK-scaffold/9 showed lower rate of growth than HHK-scaffold/1 + 32 h and HHK-scaffold/5 + 16 h during this stage. Then the SR increased slower and reached to equilibrium

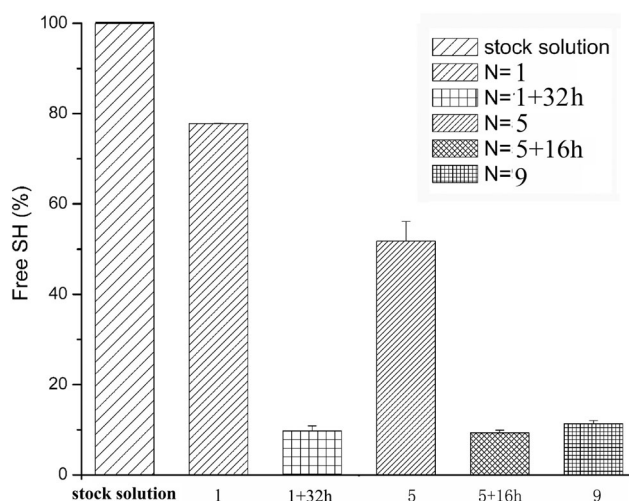


FIGURE 3. Thiol groups of the HHK stock solution and HHK samples after different freeze-thaw treatments. "N" represents the times of the freeze-thaw cycles. Data are presented as mean \pm standard deviation ($n = 3$).

after 16 h. The equilibrium value of SR was about 550% for HHK-scaffold/1 + 32 h, 480% for HHK-scaffold/5 + 16 h, and 460% for HHK-scaffold/9. This phenomenon that the SR decreased with increasing the freeze-thaw cycles could still be observed even after cell culturing for 28 days within these scaffolds [Figure 4(B)].

Porosity of the HHK scaffolds

The measured data of porosity of the HHK scaffolds are listed in Table I. As the time of freeze-thaw cycles increased, the porosity of the HHK scaffolds decreased. It is noteworthy that even at the highest number of cycles, the samples still exhibited a porosity of more than 90%, confirming that highly porous structures were achieved in all the three groups of scaffolds.

Thermal stability

Figure 5 shows the thermogravimetric curves of the scaffolds. The initial weight loss at 90–120°C was due to

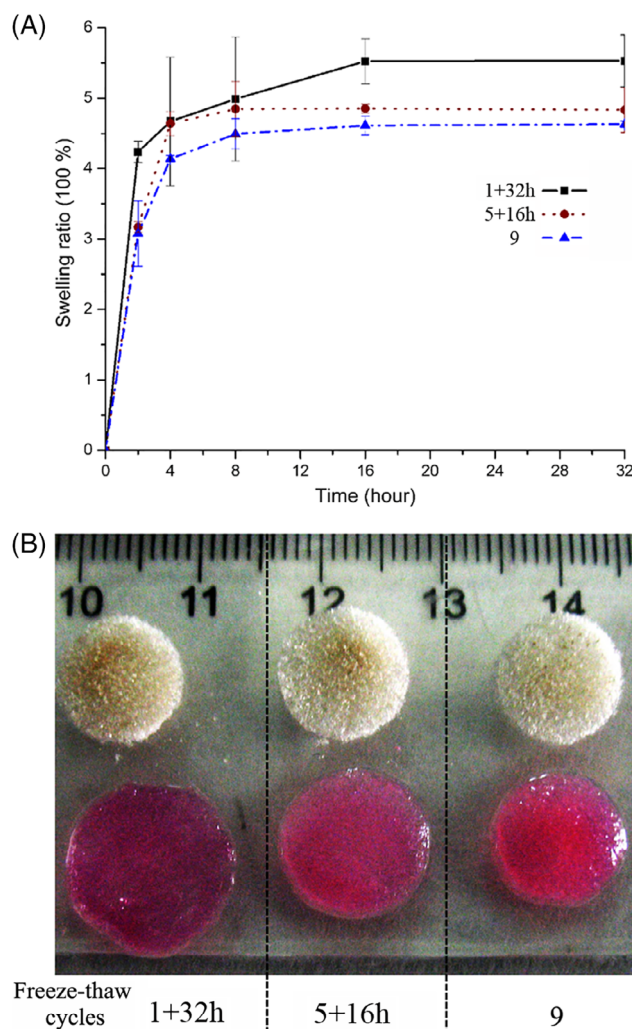


FIGURE 4. (A) Swelling behavior of HHK-scaffold/1 + 32 h, HHK-scaffold/5 + 16 h, and HHK-scaffold/9. (B) Macroscopic observation of HHK-scaffolds after cell culturing for 28 days. "N" represents the times of the freeze-thaw cycles. Data are presented as mean \pm standard deviation ($n = 5$).

TABLE I. Porosity of the HHK-Scaffold/1 + 32 h, HHK-Scaffold/5 + 16 h, and HHK-Scaffold/9

Freeze–Thaw Cycles	1 + 32 h	5 + 16 h	9
Porosity (%)	94.33 ± 0.56	92.37 ± 0.27	90.32 ± 0.49

moisture evaporation. It is concluded that moisture content of HHK-scaffold/9 was lower than that of HHK-scaffold/1 + 32 h and HHK-scaffold/5 + 16 h. The second weight loss of about 42% in all HHK scaffolds at 200–400°C was resulted from helical denaturation and decomposition of keratins.³⁵ Notably, the initial gravimetric transition temperature in this stage was different among all scaffolds and steadily elevated with increasing the number of freeze–thaw cycles, for example, 238°C for HHK-scaffold/1 + 32 h, 240°C for HHK-scaffold/5 + 16 h, and 242°C for HHK-scaffold/9, showing that HHK-scaffold/9 had a higher thermal stability than that of HHK-scaffold/5 + 16 h and HHK-scaffold/1 + 32 h. The curves tend to be stable above 400°C because of the total decomposition of HHKs.

Compressive properties

The compressive properties of the HHK scaffolds are presented in Figure 6. From Figure 6(A), the compressive modulus of HHK-scaffold/5 + 16 h was 3.15 kPa, higher than that of HHK-scaffold/1 + 32 h (2.85 kPa). However, the compressive modulus of HHK-scaffold/9 was reached to 4.52 kPa, which significantly higher than that of HHK-scaffold/5 + 16 h ($p^* < 0.05$). The compressive strength was also significantly increased ($p^* < 0.05$) with more freeze–thaw cycles [Figure 6(B)].

Microstructural imaging

From Figure 7, the pore sizes (about 100–200 μm) of scaffolds were no significantly different [Figure 7(A–C)] and the open porous structures were presented for all the three groups [Figure 7(D–F)]. It is noteworthy that some

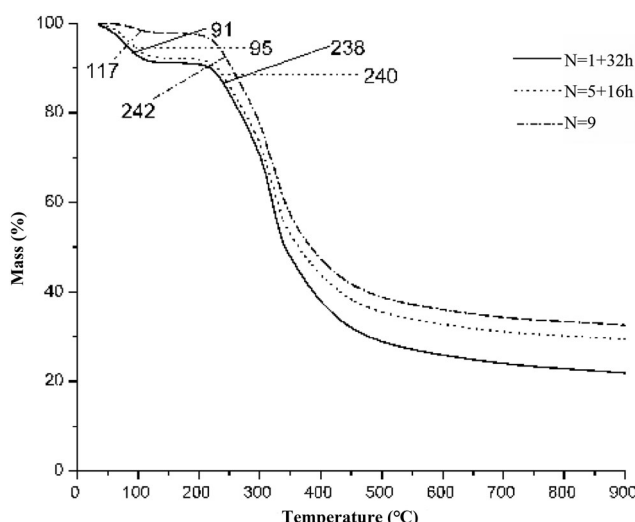


FIGURE 5. TG analyses of HHK-scaffold/1 + 32 h, HHK-scaffold/5 + 16 h, and HHK-scaffold/9. “N” represents the times of the freeze–thaw cycles.

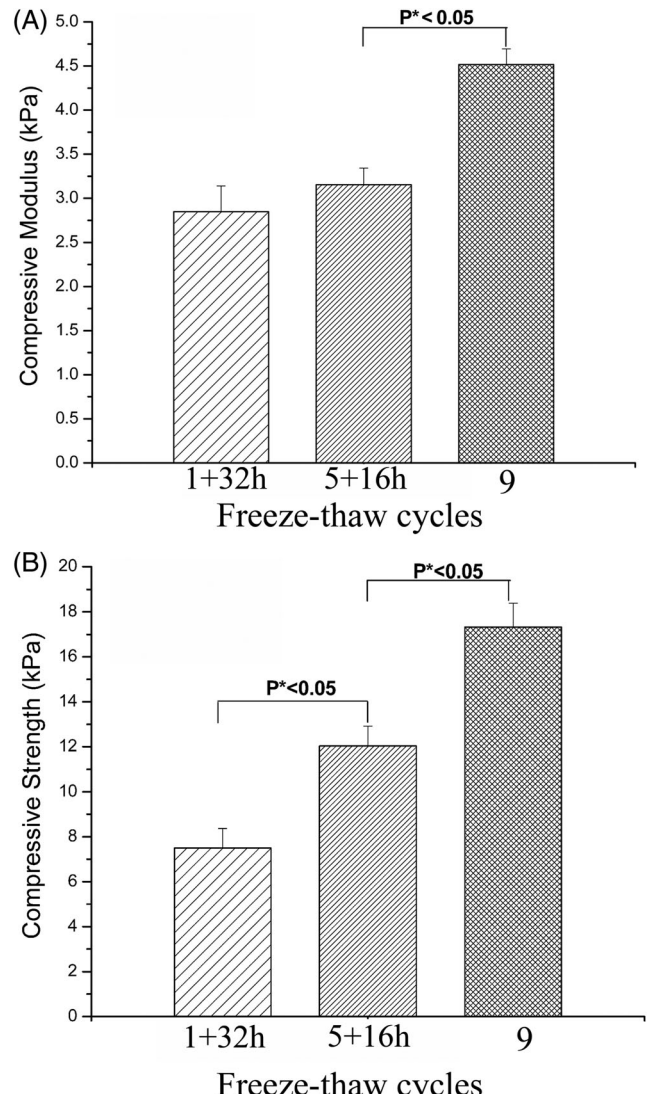


FIGURE 6. Comparison of compressive properties of three groups of HHK scaffolds: (A) compressive modulus; (B) compressive strength. “N” represents the times of the freeze–thaw cycles.

fragments which might fall out from the pore walls were exhibited in HHK-scaffold/1 + 32 h and HHK-scaffold/5 + 16 h at the higher magnification [Figure 7(A,B), blue circles]. In contrast, the similar fragments were barely observed in HHK-scaffold/9 [Figure 7(C)].

The open porous structures of the HHK scaffolds were further confirmed by using CLSM observation (Figure 8). Compared to HHK-scaffold/1 + 32 h with the inhomogeneous distribution of pores [Figure 8(A,D)], HHK-scaffold/5 + 16 h and HHK-scaffold/9 presented relatively homogeneous microstructures [Figure 8(B,E and C,F)]. The breaks which were possibly yielded by an inevitable handling to scaffolds were observed in HHK-scaffold/1 + 32 h and HHK-scaffold/5 + 16 h [Figure 8(G,H), blue arrows]. In contrast, the HHK-scaffold/9 showed a relatively intact architecture without obvious breaks [Figure 8(I)]. These results were in consistent with the SEM results of the HHK scaffolds.

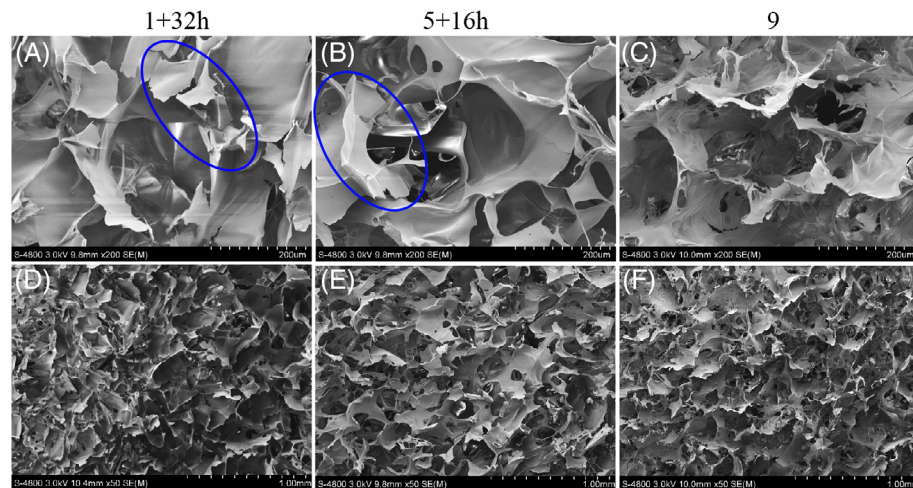


FIGURE 7. Cross-sectional SEM images of (A, D) HHK-scaffold/1 + 32 h, (B, E) HHK-scaffold/5 + 16 h, and (C, F) HHK-scaffold/9. Blue circles exhibit the fragments of the pore walls.

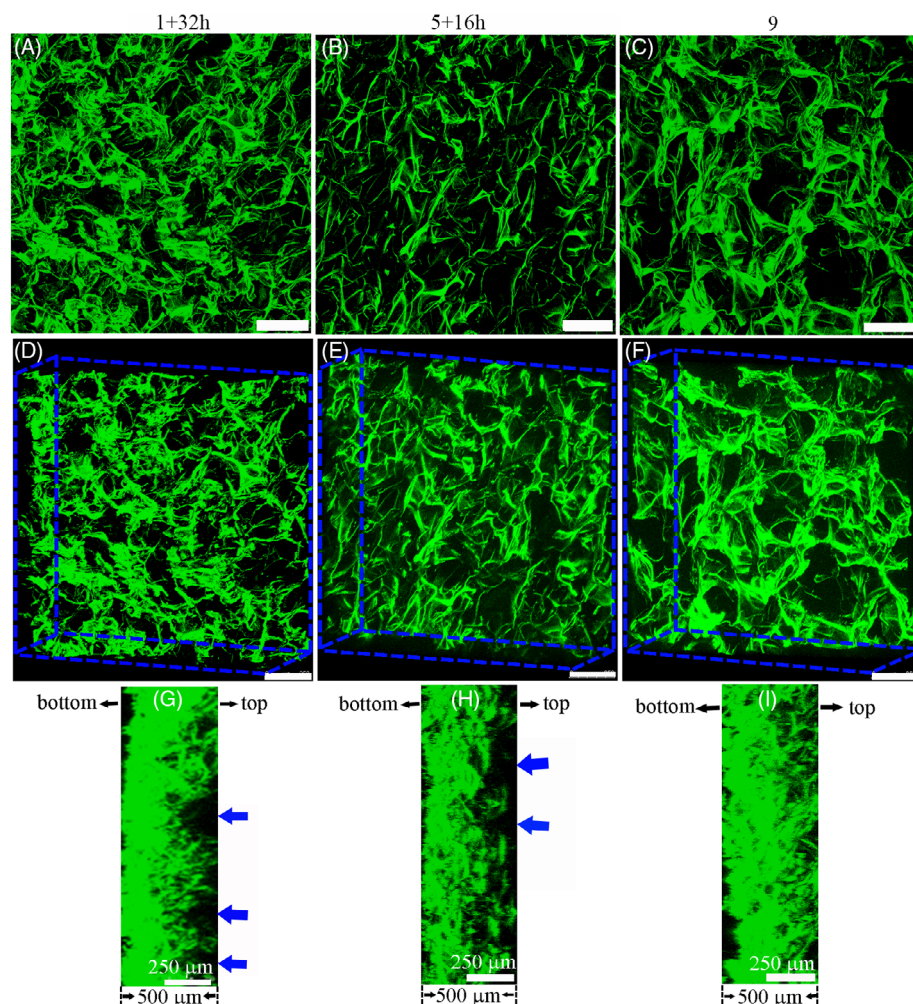


FIGURE 8. CLSM images of the HHK-scaffold/1 + 32 h (A, D, G), HHK-scaffold/5 + 16 h (B, E, H), and HHK-scaffold/9 (C, F, I). Surface micrographs (A-C) and three-dimensional micrographs (D-F; x (0°), y (90°), and z (30°); g-i: x (0°), y (90°), and z (180°)) of the HHK scaffolds at the surface and up to a depth of 500 μ m are viewed by overlaying a series of 5- μ m-thick slices along the z -axis. Blue arrows exhibit the breaks of the scaffolds.

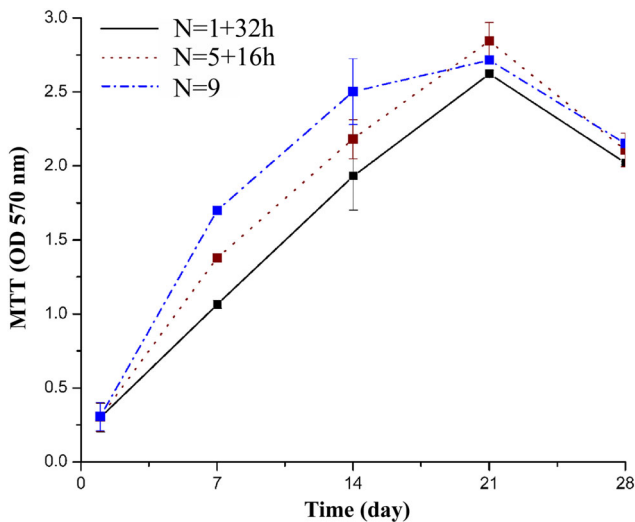


FIGURE 9. MTT results of cells cultured in the HHK scaffolds. “N” represents the times of the freeze-thaw cycles. Data are presented as the average \pm standard deviation ($n = 5$, $p < 0.05$).

Cell proliferation, attachment, and infiltration

MTT results showed that all the HHK scaffolds presented promising viability of NIH3T3 cells (Figure 9). HHK-scaffold/9 exhibited higher growth rate of cells compared with HHK-scaffold/1 + 32 h and HHK-scaffold/5 + 16 h in the first 21 days. After that, the number of cells reached to saturation density and stopped growing with contact inhibition. The number might be reduced due to factors such as nutrient depletion, accumulation of metabolites, and decreased pH in the culture medium, leading to the decreased viability.

After cell culturing for 14 days, the open porous structure of the initial cell-free HHK-scaffold/1 + 32 h was lost and most of the pore walls was collapsed [Figure 10(A,D)].

Accordingly, most of the cells migrated along the surface from the collapse pore wall and covered the whole surface of the HHK-scaffold/1 + 32 h [Figure 10(D)]. In contrast, open porous structures were still existed on HHK-scaffold/5 + 16 h and HHK-scaffold/9 [Figure 10(B,C)] and supporting the growth of cells. In Figure 10(E,F), cells migrated underneath and formed multicellular networks according to the three-dimensional microstructure of HHK-scaffold/5 + 16 h and HHK-scaffold/9.

At day 28 of cell culturing, the max-depth of cell infiltrated into the scaffolds was measured by CLSM and the value away from the top surface was about 200, 300, and 500 μm , respectively, for the HHK-scaffold/1 + 32 h, HHK-scaffold/5 + 16 h, and HHK-scaffold/9. These results indicated that cell infiltrated into the deeper scaffolds obtained with the more freeze-thaw cycles. Meanwhile, the porous three-dimensional structures remained in a relatively integrated state in all the scaffolds, which guaranteed the good attachment, proliferation, and infiltration of cells cultured in the obtained scaffolds (Figure 11).

DISCUSSION

In this study, the scaffolds are enhanced by both chemical and physical cross-links. The amount of disulfide bonds influences the chemical cross-link density of these scaffolds. Different from other proteins, keratins are rich in -SH due to a high content (about 10%) of cysteine in their domains.¹³ From Figure 3, a large quantity of free -SH groups were still presented in HHK-gel/1 and HHK-gel/5. When the thawing time prolonged, the amounts of free -SH were significantly decreased. Therefore, the amount of disulfide bonds produced in the process was dependent upon the total thaw time but not the cycles. Increasing total thaw time was necessary in the present strategy to ensure that the most of the

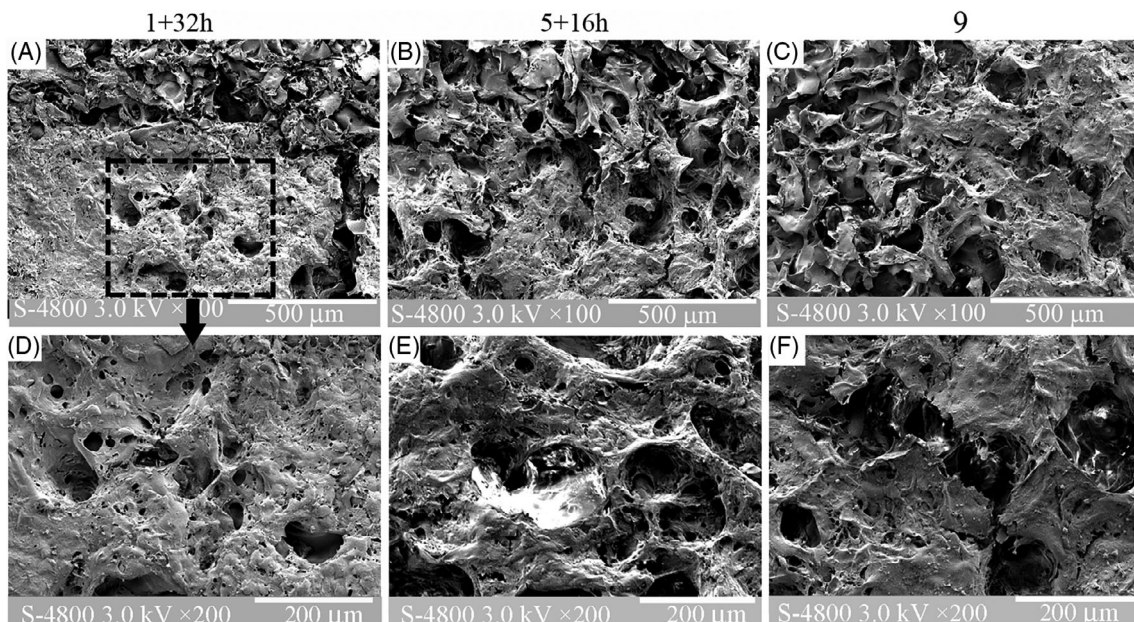


FIGURE 10. SEM images of the cell-loaded scaffolds at 14 days of cell culturing: (A, D) HHK-scaffold/1 + 32 h; (B, E) HHK-scaffold/5 + 16 h; (C, F) HHK-scaffold/9.

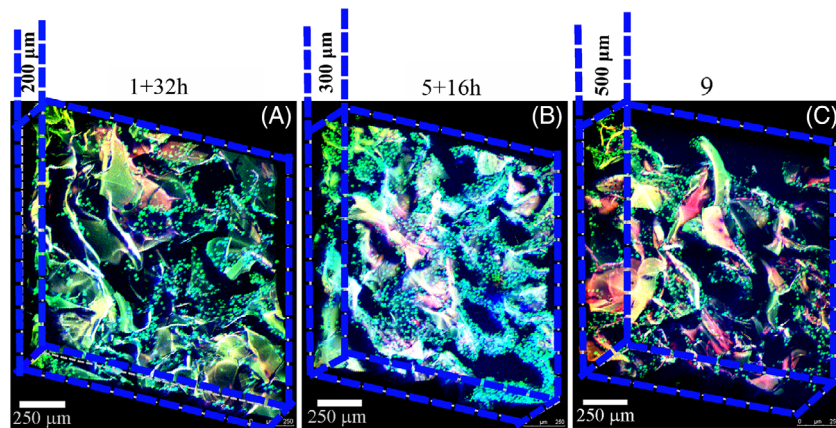


FIGURE 11. CLSM images of HHK-scaffold after cell culturing for 28 days: (A) HHK-scaffold/1 + 32 h, (B) HHK-scaffold/5 + 16 h, and (C) HHK-scaffold/9. Three-dimensional micrographs [(A–C): x (0°), y (90°), and z (30°)] of the cell-cultured scaffolds with cells infiltrated from the surface to the max-depth of the scaffolds were obtained by overlaying a series of 5- μm -thick slices along the z-axis.

-SH groups were oxidized to disulfide bonds in all samples. The physical cross-linking, such as hydrogen bonding, Van der Waals force, ionic interaction, and hydrophobic interaction,²⁹ also have a significant impact on the properties. Among these interactions, hydrogen bonding is a dominant factor in intermolecular links which can directionally cause physical cross-links from polysaccharides during cyclic freeze–thaw processes.³⁶ During the freeze stage, crystallization of the water at the low temperature could contribute to the phase separation that squeezes polymer chains close to each other. This process can facilitate the formation of hydrogen bonds with such $-\text{OH}$, $-\text{NH}_2$, and $>\text{C=O}$ groups presented in polymer chains.³⁷ As shown in Figure 2, the gelation of HHK solutions was accelerated with the equivalent total thaw time but increased freeze–thaw cycles, indicating that physical cross-links, primarily hydrogen bonds, play a vital role in the morphology transition of the HHK solution. Thus, a freeze–thaw cycle process should be helpful to promote the formation of hydrogen bonds and the self-cross-linking of keratins can be achieved by the formation of both hydrogen bonds and disulfide bonds (Figure 1). In addition, the formation process was uncontrollable because of random intramolecular and intermolecular interactions. Here, it is conjectured that the freeze–thaw cycles compel the HHK chains getting close to each other and this nonhomogeneous aggregation favorably facilitate the formation of the self-cross-linking networks.

Therefore, we expected that the scaffolds lyophilized from the HHK solutions after nine freeze–thaw cycles might possess the highest amount of the physical cross-links, primarily hydrogen bonds, among the samples treated in the current strategy while no significant difference was recorded in the amount of disulfide bonds in all the scaffolds. This speculation could be confirmed by analyzing the associated properties of all the HHK scaffolds, such as swelling behavior, porosity, thermal stability, compressive strength, and microstructural integrity (Figures 4–8 and Table I). According to thermogravimetric data (Figure 5), the thermal stability of the HHK scaffolds elevated along with increasing the freeze–thaw cycles. As the enhanced thermal stability of

macromolecules is arisen from the strong intermolecular interactions,³⁸ the intermolecular interactions of the HHK-scaffold/9 were supposed to be stronger than both HHK-scaffold/1 + 32 h and HHK-scaffold/5 + 16 h. Therefore, it is concluded that the highest physical cross-links, primarily the highest number of hydrogen bonds, among the HHK chains were achieved in the HHK-scaffold/9. Furthermore, the results of SR and porosity were in accordance with this TGA conclusion. Basically, the increased cross-links could result in the more compact structure of the processed materials with decreased SR and porosity.^{39,40} In this article, the SR and porosity of the HHK scaffolds decreased with increasing the freeze–thaw cycles (Figure 4 and Table I).

Thanks to the higher degree of cross-linking, the HHK-scaffold/9 exhibited better mechanical properties compared with HHK-scaffold/1 + 32 h and HHK-scaffold/5 + 16 h, which was illustrated by the compression test (Figure 6). As the scaffolds with high compressive strength can improve the potential of resisting stress, the HHK-scaffold/9 presented intact porous structures in comparison with the HHK-scaffold/1 + 32 h and HHK-scaffold/5 + 16 h (Figures 7 and 8). It was speculated that the fragments from the cracked pore walls might block the initial open porous structures and accordingly reduce the interconnectivity of the HHK-scaffold/1 + 32 h and HHK-scaffold/5 + 16 h. Appropriate interconnectivity with the open micropores can promote cell proliferation and penetration into the inner part of scaffolds,^{41,42} and hence the preferable cell growth rate and cell infiltration depth are observed on the HHK-scaffold/9 (Figures 8 and 9). The porous structures of all the HHK scaffolds after cell culturing for 14 days at dry state (Figure 10) were different with its initial microstructure (Figure 7). In particular, the collapsed walls of scaffolds were obviously observed in the HHK-scaffold/1 + 32 h [Figure 10(A)], which may take place during the dehydration process because of the poor mechanical properties of the scaffold.⁴⁰ In contrast, the porous three-dimensional structure was maintained for all the HHK scaffolds in the hydrated status even after cell culturing for 28 days (Figure 11). In any case, the stability of microstructures of the HHK-scaffold/9 was persistent in

comparison with that of HHK-scaffold/1 + 32 h and the HHK-scaffold/5 + 16 h.

The cell adhesion sequences, such as the RGD and LDV in the keratin chains, are barely damaged during the freeze-thaw cycles and play a key role in inducing and improving cell growth.^{4,43} Based on the results of MTT assay (Figure 9), it can be seen that the cyclic freeze-thaw treatment did not affect the bioactivity of the processed HHK scaffolds, and the cells on HHK-scaffold/9 even achieved a highest proliferation rate on 7 and 14 days. Benefited from the interconnected open porous microstructure, the highest max-depth of cell infiltration into the scaffolds was measured in HHK-scaffold/9 compared with other groups (Figure 11). Therefore, the freeze-thaw treatment is an effective technique for promoting cell proliferation, attachment, and infiltration within the HHK scaffolds.

Above all, the multiple freeze-thaw process was likely to act as an admirable approach to generate the stable microstructure of scaffolds by enhancing physically cross-linking networks in combination with the disulfide bonding networks. In the absence of cross-linking agents and organic solvents which may cause potential biotoxicity, the freeze-thaw technique is a favorable green and simple approach to prepare the mechanically robust HHK biomaterials, thus permitting the full exploitation of the unique biological performance of pure keratin materials other than keratin-based materials with other biopolymers.

CONCLUSIONS

The freeze-thaw technique provided a green and simple approach without adding extraneous reagents for the fabrication of mechanically robust pure HHK porous scaffolds. The sufficient self-cross-linking, which was composed of intermolecular hydrogen bonds in combination with disulfide bonds, could be achieved through increasing freeze-thaw cycles and as a result, improve the swelling resistance, thermal stability, and mechanical properties of the HHK scaffolds. These reinforced properties might contribute to cell proliferation, attachment, and infiltration within the HHK scaffolds. The freeze-thaw technique could be further developed as an efficient method for the fabrication of keratin-based biomaterials, so as to advance their applications in biomedical fields.

REFERENCES

1. Rogers GE. Genes for hair and avian keratins. *Ann N Y Acad Sci* 1985;455(1):403–425.
2. Tachibana A, Furuta Y, Takeshima H, Tanabe T, Yamauchi K. Fabrication of wool keratin sponge scaffolds for long-term cell cultivation. *J Biotechnol* 2002;93(2):165–170.
3. Verma V, Verma P, Ray P, Ray AR. Preparation of scaffolds from human hair proteins for tissue-engineering applications. *Biomed Mater* 2008;3(2):025007.
4. Sierpinski P, Garrett J, Ma J, Apel P, Klorig D, Smith T, Koman LA, Atala A, Van Dyke M. The use of keratin biomaterials derived from human hair for the promotion of rapid regeneration of peripheral nerves. *Biomaterials* 2008;29(1):118–128.
5. Xu S, Sang L, Zhang Y, Wang X, Li X. Biological evaluation of human hair keratin scaffolds for skin wound repair and regeneration. *Korean J Couns Psychother* 2013;33(2):648–655.
6. Yao CH, Lee CY, Huang CH, Chen YS, Chen KY. Novel bilayer wound dressing based on electrospun gelatin/keratin nanofibrous mats for skin wound repair. *Korean J Couns Psychother* 2017;79:533–540.
7. Aboushwareb T, Eberli D, Ward C, Broda C, Holcomb J, Atala A, Van Dyke M. A keratin biomaterial gel hemostat derived from human hair: Evaluation in a rabbit model of lethal liver injury. *J Biomed Mater Res B Appl Biomater* 2009;90(1):45–54.
8. Rahmany MB, Hantgan RR, Van Dyke M. A mechanistic investigation of the effect of keratin-based hemostatic agents on coagulation. *Biomaterials* 2013;34(10):2492–2500.
9. Luo T, Hao S, Chen X, Wang J, Yang Q, Wang Y, Weng Y, Wei H, Zhou J, Wang B. Development and assessment of keratine nanoparticles for use as a hemostatic agent. *Korean J Couns Psychother* 2016;63:352–358.
10. Sun Z, Yi Z, Zhang H, Ma X, Su W, Sun X, Li X. Bio-responsive alginate-keratin composite nanogels with enhanced drug loading efficiency for cancer therapy. *Carbohydr Polym* 2017;175:159–169.
11. Yi Z, Sun Z, Chen G, Zhang H, Ma X, Su W, Cui X, Li X. Size-controlled, colloidally stable and functional nanoparticles based on the molecular assembly of green tea polyphenols and keratins for cancer therapy. *J Mater Chem B* 2018;6(9):1373–1386.
12. Sun Z, Yi Z, Cui X, Chen X, Su W, Ren X, Li X. Tumor-targeted and nitric oxide-generated nanogels of keratin and hyaluronan for enhanced cancer therapy. *Nanoscale* 2018;10(25):12109–12122.
13. Rouse JG, Van Dyke ME. A review of keratin-based biomaterials for biomedical applications. *Materials (Basel)* 2010;3(2):999–1014.
14. Vasconcelos A, Cavacapulo A, Cavacapulo A. The use of keratin in biomedical applications. *Curr Drug Targets* 2013;14(5):612–619.
15. Katoh K, Tanabe T, Yamauchi K. Novel approach to fabricate keratin sponge scaffolds with controlled pore size and porosity. *Biomaterials* 2004;25(18):4255–4262.
16. Scalfaro R, Lopresti F, Botta L, Rigogliuso S, Ghersi G. Preparation of three-layered porous PLA/PEG scaffold: Relationship between morphology, mechanical behavior and cell permeability. *J Mech Behav Biomed Mater* 2016;54:8–20.
17. Wang X, Sang L, Luo D, Li X. From collagen-chitosan blends to three-dimensional scaffolds: The influences of chitosan on collagen nanofibrillar structure and mechanical property. *Colloids Surf B Biointerfaces* 2011;82(1):233–240.
18. Su W, Ma X, Sun Z, Yi Z, Cui X, Chen G, Chen X, Guo B, Li X. RhBMP-2 and concomitant rapid material degradation synergistically promote bone repair and regeneration with collagen-hydroxyapatite nanocomposites. *J Mater Chem B* 2018;6(26):4338–4350.
19. Balaji S, Kumar R, Sriprya R, Kakkar P, Ramesh DV, Reddy PNK, Sehgal PK. Preparation and comparative characterization of keratin-chitosan and keratin-gelatin composite scaffolds for tissue engineering applications. *Mater Sci Eng C* 2012;32(4):975–982.
20. Ramadoss P, Thanigai Arul K, Ramana Ramya J, Rigana Begam M, Sarath Chandra V, Manikandan E. Enhanced mechanical strength and sustained drug release of gelatin/keratin scaffolds. *Mater Lett* 2017;186:109–112.
21. Tu H, Yu R, Lin Z, Zhang L, Lin N, Yu WD, Liu XY. Programming performance of wool keratin and silk fibroin composite materials by mesoscopic molecular network reconstruction. *Adv Funct Mater* 2016;26(48):9032–9043.
22. Vasconcelos A, Freddi G, Cavaco-Paulo A. Biodegradable materials based on silk fibroin and keratin. *Biomacromolecules* 2008;9(4):1299–1305.
23. Tanabe T, Okitsu N, Tachibana A, Yamauchi K. Preparation and characterization of keratin-chitosan composite film. *Biomaterials* 2002;23(3):817–825.
24. Silva R, Singh R, Sarker B, Papageorgiou DG, Juhasz JA, Roether JA, Cicha I, Kaschta J, Schubert DW, Chrissafis K and others. Hybrid hydrogels based on keratin and alginate for tissue engineering. *J Mater Chem B* 2014;2(33):5441–5451.
25. Hartrianti P, Nguyen LTH, Johanes J, Chou SM, Zhu P, Tan NS, Tang MBY, Ng KW. Fabrication and characterization of a novel crosslinked human keratin-alginate sponge. *J Tissue Eng Regen Med* 2017;11(9):2590–2602.
26. Tanabe T, Okitsu N, Yamauchi K. Fabrication and characterization of chemically crosslinked keratin films. *Mater Sci Eng C* 2004;24(3):441–446.

27. Dou Y, Huang X, Zhang B, He M, Yin G, Cui Y. Preparation and characterization of a dialdehyde starch crosslinked feather keratin film for food packaging application. *RSC Adv* 2015;5(34):27168–27174.
28. Cui L, Gong J, Fan X, Wang P, Wang Q, Qiu Y. Transglutaminase-modified wool keratin film and its potential application in tissue engineering. *Eng Life Sci* 2013;13(2):149–155.
29. Cai Z, Zhang F, Wei Y, Zhang H. Freeze-thaw-induced gelation of hyaluronan: Physical cryostructuring correlated with intermolecular associations and molecular conformation. *Macromolecules* 2017;50(17):6647–6658.
30. Otsuka E, Suzuki A. A simple method to obtain a swollen PVA gel crosslinked by hydrogen bonds. *J Appl Polym Sci* 2009;114(1):10–16.
31. Schrooyen PM, Dijkstra PJ, Oberthür RC, Bantjes A, Feijen J. Partially carboxymethylated feather keratins. 1. Properties in aqueous systems. *J Agric Food Chem* 2000;48(9):4326–4334.
32. Wang S, Wang Z, Foo SE, Tan NS, Yuan Y, Lin W, Zhang Z, Ng KW. Culturing fibroblasts in 3D human hair keratin hydrogels. *ACS Appl Mater Interfaces* 2015;7(9):5187–5198.
33. Bulaj G, Kortemme T, Goldenberg DP. Ionization–reactivity relationships for cysteine thiols in polypeptides. *Biochemistry* 1998;37(25):8965–8972.
34. Xu H, Cai S, Xu L, Yang Y. Water-stable three-dimensional ultrafine fibrous scaffolds from keratin for cartilage tissue engineering. *Langmuir* 2014;30(28):8461–8470.
35. Spei M, Holzemer R. Thermoanalytical investigations of extended and annealed keratins. *Colloid Polym Sci* 1987;265(11):965–970.
36. Zhang H, Zhang F, Wu J. Physically crosslinked hydrogels from polysaccharides prepared by freeze–thaw technique. *React Funct Polym* 2013;73(7):923–928.
37. Peppas NA, Stauffer SR. Reinforced uncrosslinked poly (vinyl alcohol) gels produced by cyclic freezing–thawing processes: A short review. *J Control Release* 1991;16(3):305–310.
38. Kweon H, Um IC, Park YH. Structural and thermal characteristics of *Antheraea pernyi* silk fibroin/chitosan blend film. *Polymer* 2001;42(15):6651–6656.
39. Xiao C, Yang M. Controlled preparation of physical cross-linked starch-g-PVA hydrogel. *Carbohydr Polym* 2006;64(1):37–40.
40. Sang L, Luo D, Xu S, Wang X, Li X. Fabrication and evaluation of biomimetic scaffolds by using collagen-alginate fibrillar gels for potential tissue engineering applications. *Mater Sci Eng C* 2011;31(2):262–271.
41. Chen G, Ushida T, Tateishi T. Scaffold design for tissue engineering. *Macromol Biosci* 2002;2(2):67–77.
42. Mandal BB, Kundu SC. Non-mulberry silk gland fibroin protein 3-D scaffold for enhanced differentiation of human mesenchymal stem cells into osteocytes. *Acta Biomater* 2009;5(7):2579–2590.
43. Tachibana A, Kaneko S, Tanabe T, Yamauchi K. Rapid fabrication of keratin–hydroxyapatite hybrid sponges toward osteoblast cultivation and differentiation. *Biomaterials* 2005;26(3):297–302.